PERGAMON

International Journal of Solids and Structures 38 (2001) 4265–4278

INTERNATIONAL JOURNAL OF SOLIDS and STRUCTURES

www.elsevier.com/locate/ijsolstr

Birdcaging and the collapse of rods and cables in fixed-grip compression

D.M. Stump [a], G.H.M. van der Heijden [b,*]

[a] *Department of Mathematics, University of Queensland, St. Lucia QLD 4072, Australia*
[b] *Centre for Nonlinear Dynamics, University College London, Gower Street, London WC1E 6BT, UK*

Received 12 December 1999; in revised form 22 June 2000

Abstract

Wound cables and straight rods exhibit lateral instabilities when loaded under compression and rotation in fixed-grip conditions. In a multi-strand cable made from helically wound strands, this produces a "bird cage" structure where the constituent strands separate to leave a central void region. For a straight rod, a similar instability occurs when the planar elastica becomes unstable under significant axial compression. The large deflection theory of linear elastic rods is used to explain these behaviours in terms of the standard concepts of the theory of buckling, post-buckling, and imperfection sensitivity. The problem provides an excellent vehicle for the use of Euler parameters (quaternions) which remove the singularities normally associated with an Euler angle formulation.

Keywords: Birdcaging; Wound cable; Lateral instability; Post-buckling behaviour; Imperfection sensitivity; Euler parameters; Perturbation analysis

1. Introduction

Multi-strand wound cables which are subject to twist counter to the direction of strand winding and are then loaded in compression can undergo a phenomenon termed "birdcaging" where the strands open up to leave a central void surrounded by a complex of strands. It is not hard to simulate this effect by winding together two strands of rope to form a cable and then using your hands to apply the load described above. Once the bird cage reaches a certain size, the force necessary to compress the two ends drops significantly with their inward motion so that the cable collapses under the application of a fixed load. A similar type of collapse behaviour can be seen during the axial compression of an initially straight rod such as a piece of piano wire. If the ends are held in fixed-grip boundary conditions with prescribed position, tangent, and rotation, then the rod first buckles into a planar elastica. The continued compression of the rod under increasing force eventually produces an out-of-plane buckling at which point further inward compression

* Corresponding author.
E-mail address: g.heijden@ucl.ac.uk (G.H.M. van der Heijden).

0020-7683/01/$ - see front matter
PII: S0020-7683(00)00275-4

occurs under a dropping load so that the rod collapses. An important industrial example of this lateral instability is that occurring in underwater towing cables (Nair and Hegemeier, 1979).

The objective of this paper is to present a theory explaining this phenomenon in both helically wound cables and in straight rods. The wound cable can be viewed as consisting of a series of imperfect straight rods so that the loading behaviour can be explained, at least approximately, in terms of many of the standard concepts of the buckling and post-buckling theories of rods.

Much of the previous work on the lateral buckling problem has been restricted to the study of linear equations for the beam. The problem with this approach is that the beam may undergo a large symmetric deflection before it becomes unstable. Nonlinear studies have been conducted by Kovári (1969), who considers the case of an isotropic rod free to twist at one end, Maddocks (1984), who considers bifurcation under several types of boundary conditions in dead load using variational methods, and Antman (1984), who studies the linearization of the nonlinear equations about a planar solution.

The nonlinear large-deflection theory of elastic rods has been applied to twisted wire cables by Phillips and Costello (1973), but they consider a situation where the strands of the deformed cable remain helical in shape. (See also Costello (1978) for a review of work on wound cables.) The birdcaging phenomenon is explicitly studied by Conway and Costello (1990), who consider a set of two coupled linear partial differential equations that also model the dynamics of the problem, but are only valid for small deflections. In the present paper, we study birdcaging within a large-deflection formulation, which to the best of our knowledge has not been done before. We do not make any assumptions on the shape of the rod; rather, the bird cage shape comes out of the full nonlinear theory by applying the right boundary conditions.

Conventional formulations for determining the buckling load and mode shape in terms of Euler angles are problematic since the elastica solution goes through polar singularities at specific points along its length. Recently, Miyazaki and Kondo (1997) have studied numerical and analytical aspects of this buckling point for isotropic cross-sectional rods by reparameterizing the problem and using one of the Euler angles rather than the arc-length as the independent variable. The isotropic cross-section rod represents a special case mathematically because the system is completely integrable given the proper constitutive behaviour. However, lateral instability also occurs in anisotropic cross-section rods, which in general do not have an integrable system of equations. Neither, for that matter, do the rods with initial curvature that constitute the strands of the wound cable (Champneys et al., 1997). Part of the objective here is to develop a perturbation approach that can describe the lateral buckling and post-buckling behaviour for linear elastic rods with arbitrary cross-sectional properties, including tapes. The simulation of the helically wound cable is primarily computational in form; however, the buckling and post-buckling analyses for the straight rod can be carried a significant distance analytically. (For simplicity, a wound cable made up of isotropic strands will be considered. It is not a particularly useful exercise to extend the analysis to a wound cable made from strands with anisotropic cross-sections, although this can be done in principle.)

The lateral buckling of the straight rod and the collapse behaviour of the wound cable both afford an excellent opportunity to exploit the power of Euler parameter (quaternion) rather than traditional Euler angle formulations. As discussed by Kehrbaum and Maddocks (1997), the use of Euler parameters removes the polar singularity associated with Euler angles, which can significantly improve the numerical solution of two-point boundary value problems in rods. These numerical advantages come at a price in that the canonical variables are difficult to interpret physically and that physically straightforward boundary conditions may not lead to simple conditions when expressed in the canonical variables.

The paper is organized as follows. In Section 2, the mathematical formulation of the problem is described. This includes the cases of both the straight rod and the helically wound cable. For definiteness, we will consider the case of a cable made up of two helical strands. In Section 3, the buckling and post-buckling analyses of the straight rod are conducted. The buckling behaviour is studied as a function of the anisotropy of the rod's cross-section. It is found that asymptotically for thin rods (tapes) all quantities reach finite values, and we compute these values in a suitable perturbation analysis. In Section 4, the numerical

results for the helically wound cable are assessed in terms of the imperfection sensitivity of the straight rod. Section 5 concludes the paper.

2. The mathematical formulation

2.1. The kinematic equations

The problems under consideration are shown schematically in Figs. 1 and 2 and consist of a finite-length 2-strand helical ply made from circular cross-section rods and a finite-length straight rod with an anisotropic cross-section. The two strands that make up the ply are assumed not to exert contact forces onto each other (at most merely to touch) during the entire loading sequence. This is a reasonable assumption as the initial curvature acts as an imperfection. Thus, the buckling of the cable is destroyed and the strands break contact the instant the cable is compressed or a rotation counter to the winding direction is applied. This is also confirmed by simple experiments with short pieces of made-up cable. Therefore, the description of the ply can be restricted to one of the strands, the other one just being a rotated copy of the first. The centre lines of the rods (either one of the strands in the ply or the straight rod) are described by position vectors $\mathbf{r}(s)$ measured from the origins O of the Cartesian coordinate systems indicated in the figures.

The two figures use different orientations of the coordinate systems for the stress-free reference configurations. The reasons for these particular choices are discussed below. Of course, the theory can be reformulated using the same orientation for both problems, if one so choses. In both problems, the rods are assumed to be inextensible and to deform in a symmetric manner so that the arc-length coordinate s lies in the range $0 \leqslant s \leqslant L$, where L is half the length of the rod.

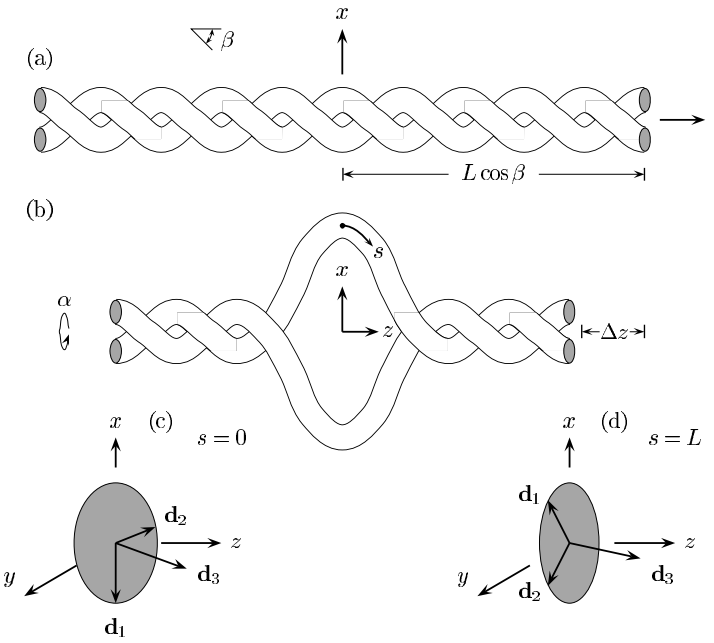

Fig. 1. A 2-strand wound cable: (a) relaxed configuration, (b) bird cage formation under axial compression Δz and counter rotation α, (c) the material and Cartesian axes systems at $s = 0$, and (d) the axes systems at $s = L$.

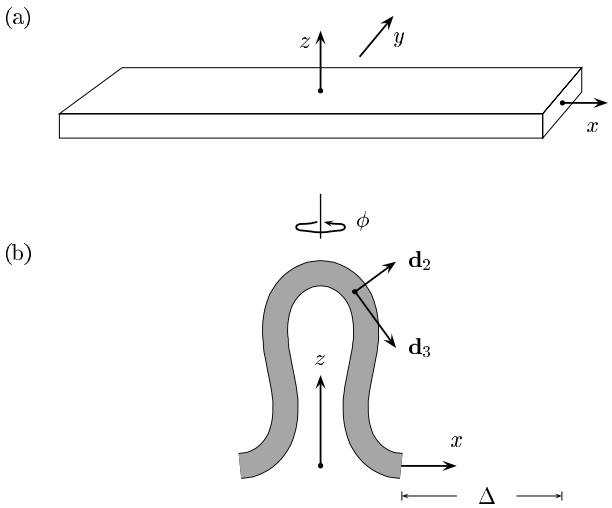

Fig. 2. The nonisotropic cross-section rod: (a) general view of coordinate system, and (b) the planar shape at the critical compression with the ϕ rotation of the buckling mode indicated. (Euler angle orientations can be deduced from the $\mathbf{d}_2$ and $\mathbf{d}_3$ axes.)

The Frenet basis vectors $\mathbf{r}'$, $\mathbf{n} = \mathbf{r}''/|\mathbf{r}''|$, and $\mathbf{b} = \mathbf{r}' \times \mathbf{n}$, where $(\ )'$ denotes differentiation with respect to the arc-length coordinate s, are sufficient to describe the configuration of the isotropic cross-section rod. In order to model the orientation of the anisotropic rod, the material basis vectors ($\mathbf{d_1}$, $\mathbf{d_2}$, $\mathbf{d_3}$) are introduced, where $\mathbf{d_3} = \mathbf{r}'$ and the vectors $\mathbf{d}_1$ and $\mathbf{d}_2$ describe the principal inertia directions within the cross-section. The material basis vectors are parameterized in terms of the three Euler angles θ, ϕ and ψ by the formulas (Landau and Lifshitz, 1963)

$$\begin{cases} \mathbf{d}_1 = (\cos\psi\cos\phi - \sin\psi\cos\theta\sin\phi)\mathbf{i} + (\cos\psi\sin\phi + \sin\psi\cos\theta\cos\phi)\mathbf{j} + \sin\psi\sin\theta\,\mathbf{k}, \\ \mathbf{d}_2 = -(\sin\psi\cos\phi + \cos\psi\cos\theta\sin\phi)\mathbf{i} + (-\sin\psi\sin\phi + \cos\psi\cos\theta\cos\phi)\mathbf{j} + \cos\psi\sin\theta\,\mathbf{k}, \\ \mathbf{d}_3 = \sin\theta\sin\phi\,\mathbf{i} - \sin\theta\cos\phi\,\mathbf{j} + \cos\theta\,\mathbf{k}. \end{cases} \tag{1}$$

The derivatives of the Euler angles are related to the material basis components of the curvature vector $\mathbf{u}$ by the equations

$$\theta' = u_1\cos\psi - u_2\sin\psi, \qquad \phi' = \frac{u_1\sin\psi + u_2\cos\psi}{\sin\theta}, \qquad \psi' = u_3 - \phi'\cos\theta. \tag{2}$$

The equation for ϕ' contains the polar singularity.

An alternative parameterization (Junkins and Turner, 1986) of the rod centre line is in terms of four Euler parameters (b_0, b_1, b_2, b_3) which form the components of a quaternion and satisfy the constraint

$$b_0^2 + b_1^2 + b_2^2 + b_3^2 = 1.$$

The Euler parameters are related to the Euler angles by the trigonometric expressions

$$\begin{cases} b_0 = \cos\frac{\theta}{2}\cos\frac{1}{2}(\phi+\psi), & b_1 = \sin\frac{\theta}{2}\cos\frac{1}{2}(\phi-\psi), \\ b_2 = \sin\frac{\theta}{2}\sin\frac{1}{2}(\phi-\psi), & b_3 = \cos\frac{\theta}{2}\sin\frac{1}{2}(\phi+\psi). \end{cases} \tag{3}$$

The parameterization of the material basis vectors in terms of the Euler parameters becomes

$$\mathbf{d}_1 = (b_0^2 + b_1^2 - b_2^2 - b_3^2)\mathbf{i} + 2(b_1b_2 + b_0b_3)\mathbf{j} + 2(b_1b_3 - b_0b_2)\mathbf{k}, \tag{4a}$$

$$\mathbf{d}_2 = 2(b_1b_2 - b_0b_3)\mathbf{i} + (b_0^2 - b_1^2 + b_2^2 - b_3^2)\mathbf{j} + 2(b_2b_3 + b_0b_1)\mathbf{k}, \tag{4b}$$

$$\mathbf{d}_3 = 2(b_1b_3 + b_0b_2)\mathbf{i} + 2(b_2b_3 - b_0b_1)\mathbf{j} + (b_0^2 - b_1^2 - b_2^2 + b_3^2)\mathbf{k}, \tag{4c}$$

while the equations relating the derivatives of the Euler parameters with the curvature vector components are

$$\begin{cases} 2b_0' = -b_1u_1 - b_2u_2 - b_3u_3, & 2b_1' = b_0u_1 - b_3u_2 + b_2u_3, \\ 2b_2' = b_3u_1 + b_0u_2 - b_1u_3, & 2b_3' = -b_2u_1 + b_1u_2 + b_0u_3. \end{cases} \tag{5}$$

The Cartesian components (x, y, z) of the position vector $\mathbf{r}$ are obtained by integrating the expressions

$$x' = 2(b_1b_3 + b_0b_2), \qquad y' = 2(b_2b_3 - b_0b_1), \qquad z' = b_0^2 - b_1^2 - b_2^2 + b_3^2, \tag{6}$$

which come from (4c).

2.1.1. Initial curvature

In order to fully model the wound cable, account must be taken of the natural helical shape of the individual constituent strands. The Cartesian position vector of an isolated strand in the stress-free reference configuration is (Fig. 1a)

$$\mathbf{r}^*(s) = \cos(s\sin\beta)\mathbf{i} + \sin(s\sin\beta)\mathbf{j} + s\cos\beta\,\mathbf{k},$$

where β is the helix angle, and the helical radius a has been used as the characteristic length. (All quantities associated with the helical reference state of the strand are denoted by a superscript $*$.) The position vector of the other strand is obtained by rotating this strand through the angle π about the $\mathbf{k}$ axis. The Frenet basis vectors are

$$\begin{cases} \mathbf{r}^{*\prime} = \sin\beta[-\sin(s\sin\beta)\mathbf{i} + \cos(s\sin\beta)\mathbf{j}] + \cos\beta\,\mathbf{k}, \\ \mathbf{n}^* = -\cos(s\sin\beta)\mathbf{i} - \sin(s\sin\beta)\mathbf{j}, \\ \mathbf{b}^* = \cos\beta[\sin(s\sin\beta)\mathbf{i} - \cos(s\sin\beta)\mathbf{j}] + \sin\beta\,\mathbf{k}. \end{cases} \tag{7}$$

A comparison of Eqs. (1) and (7) shows that the choice of

$$\theta^* = \beta, \qquad \phi^* = s\sin\beta + \pi, \qquad \psi^* = 0$$

is consistent with $\mathbf{d}_1^* = \mathbf{n}^*$, $\mathbf{d}_2^* = \mathbf{b}^*$ and $\mathbf{d}_3^* = \mathbf{r}^{*\prime}$. For an isotropic rod, ψ^* can be chosen arbitrarily, but this choice provides an alignment between the two systems. The orientation of the Cartesian coordinate system in Fig. 1 has been chosen so that the angles θ^* and ϕ^* are constant and linear functions, respectively, when the strand is in its reference configuration.

The use of Eq. (2) shows that in the stress-free reference configuration, the curvature components are

$$u_1^* = 0, \qquad u_2^* = \sin^2\beta, \qquad u_3^* = \sin\beta\cos\beta. \tag{8}$$

The components u_2^* and u_3^* are the curvature and the torsion of a helical space curve of radius one. The special case of a straight rod is obtained by taking the limit $\beta \to 0$ to obtain a rod lying in the z-direction at $x = 1$.

2.2. The equilibrium and constitutive equations

The force and moment vectors, $\mathbf{n}$ and $\mathbf{m}$, respectively, acting at the centre of the rod cross-section obey the vector equations of an end-loaded rod:

$$\mathbf{n}' = \mathbf{0} \quad \text{and} \quad \mathbf{m}' + \mathbf{r}' \times \mathbf{n} = \mathbf{0}.$$

No pressure is assumed to develop between the strands of the wound cable in either the reference configuration or the deformed shape. These two equations admit the constant integrals $|\mathbf{n}|$ and $\mathbf{m}\cdot\mathbf{n}$ regardless of the cross-sectional properties. (It is worth emphasizing that these are two constants along the length of the rod in any particular configuration. The values of these constants throughout a given deformation process depend upon the boundary conditions on the rod.) In material basis vector components, the equilibrium equations take the form

$$\begin{cases} n_1' = n_2u_3 - n_3u_2, & m_1' = m_2u_3 - m_3u_2 + n_2, \\ n_2' = n_3u_1 - n_1u_3, & m_2' = m_3u_1 - m_1u_3 - n_1, \\ n_3' = n_1u_2 - n_2u_1, & m_3' = m_1u_2 - m_2u_1, \end{cases} \tag{9}$$

where use has been made of the equations for the evolution of the basis vectors

$$\mathbf{d}_i' = \mathbf{u}\times\mathbf{d}_i \quad (i = 1,2,3).$$

The rod is taken as inextensible and linear elastic so that the components of $\mathbf{n}$ must be determined from Eq. (9) while the relationships between the moment and curvature vector components are

$$m_1 = u_1 - u_1^*, \qquad m_2 = A_2(u_2 - u_2^*), \qquad m_3 = A_3(u_3 - u_3^*). \tag{10}$$

All forces and moments have been made dimensionless with respect to the bending rigidity about the $\mathbf{d}_1$ axis so that the constants A_2 and A_3 represent dimensionless rigidities about the $\mathbf{d}_2$ and $\mathbf{d}_3$ axes. For an isotropic cross-section rod $A_2 = 1$.

The configuration of the rod is fully determined by the vector quantities ($\mathbf{r}$, $\mathbf{n}$, $\mathbf{m}$, $\mathbf{u}$) and the four Euler parameters (b_0, b_1, b_2, b_3) which obey the Eqs. (5), (6), (9), and (10).

2.3. The boundary conditions

2.3.1. Wound cable

The strands of the wound cable are assumed to deform in the manner shown in Fig. 1b under imposed axial shortening and rotation counter to the winding direction. A bird cage structure forms about the location $s = 0$ and has two-fold rotational symmetry about both the $\mathbf{i}$ and $\mathbf{k}$ axes. The boundary conditions at $s = 0$ shown in Fig. 1c are given by

$$\mathbf{r}(0) = x_0\mathbf{i}, \qquad \phi(0) = \pi, \qquad \psi(0) = 0, \qquad \theta(0) = \theta_0, \tag{11}$$

where x_0 and θ_0 are unknown. The rod is assumed to be gripped rigidly at $s = L$ so that the Euler angles $\theta(L)$ and $\psi(L)$ remain fixed in their reference configuration values (Fig. 1d) while the strand is displaced inward along the $\mathbf{k}$ axis by an amount Δz and the position and tangent vectors are rotated about this axis by an angle α in the direction counter to the winding. This leads to the six boundary conditions

$$\begin{cases} x(L) = \cos(L\sin\beta - \alpha), & y(L) = \sin(L\sin\beta - \alpha), & z(L) = L\cos\beta - \Delta z, \\ \theta(L) = \beta, & \phi(L) = L\sin\beta + \pi - \alpha, & \psi(L) = 0. \end{cases} \tag{12}$$

It is straightforward to use Eq. (3) to express the Euler angle boundary conditions in terms of Euler parameters. The problem formulation is completed by noting that at $s = 0$, the unknown force and moment vectors take the form

$$\mathbf{n}(0) = n_2^0\mathbf{d}_2 + n_3^0\mathbf{d}_3, \qquad \mathbf{m}(0) = m_2^0\mathbf{d}_2 + m_3^0\mathbf{d}_3,$$

so that the six quantities $(x_0, \theta_0, n_2^0, n_3^0, m_2^0, m_3^0)$ are used as iterates in a shooting method to satisfy the six constraints given by Eq. (12).

2.3.2. Straight rod

The boundary conditions on the initially straight rod shown in Fig. 2a are obtained in a similar manner, although there is no imposed rotation of the endpoint about the **i** axis, only an inward displacement in this direction. The configuration of the straight rod just after the instant of lateral elastica buckling is shown in Fig. 2b. The rod shape is symmetric about the **i** axis. At $s = 0$, the specified position components and Euler angles are

$$x(0) = y(0) = 0, \qquad \theta(0) = \pi/2, \qquad \psi(0) = 0, \tag{13}$$

while the angle $\phi(0)$ is $\pi/2$ prior to buckling, but is unknown once buckling has occurred. The specified position and boundary conditions at $s = L$ are

$$y(L) = z(L) = 0, \qquad \theta(L) = \pi/2, \qquad \phi(L) = \pi/2, \qquad \psi(L) = 0, \tag{14}$$

while the value of the critical compression $\Delta = L - x(L)$ at the instant of buckling must be determined by simultaneously computing the buckling mode.

It should be noted that for both the wound cable and the straight rod, there are some first integrals that allow us to reduce the size of the problem (Kehrbaum and Maddocks, 1997). However, the imposition of the boundary conditions in either the forms (11) and (12) or (13) and (14), is most easily accomplished numerically without attempting to partially integrate the system of equations.

3. Buckling of the straight rod

The elastica solution of the compressed straight rod is a canonical problem of large deflection linear elasticity (Love, 1927) and the solution can be expressed entirely in terms of elliptic integrals and Jacobi elliptic functions. The planar solution involves bending only about the $\mathbf{d}_1$ axis, while after the lateral buckling, there is bending about both the $\mathbf{d}_1$ and $\mathbf{d}_2$ axes and twisting about the $\mathbf{d}_3$ axis. Following the methods of buckling and post-buckling analysis discussed in Budiansky (1974), this leads to the expansion of the various quantities in the perturbation series

$$\begin{cases} x = x_0 + \epsilon^2\tilde{x} + \cdots, \quad \theta = \theta_0 + \epsilon^2\tilde{\theta} + \cdots, \\ y = \epsilon\hat{y} + \epsilon^3\bar{y} + \cdots, \quad \phi = \pi/2 + \epsilon\hat{\phi} + \epsilon^3\bar{\phi} + \cdots, \\ z = z_0 + \epsilon^2\tilde{z} + \cdots, \quad \psi = \epsilon\hat{\psi} + \epsilon^3\bar{\psi} + \cdots, \\ \\ n_1 = \epsilon\hat{n}_1^0 + \epsilon^3\bar{n}_1 + \cdots, \quad u_1 = u_1^0 + \epsilon^2\tilde{u}_1 + \cdots, \\ n_2 = n_2^0 + \epsilon^2\tilde{n}_2 + \cdots, \quad u_2 = \epsilon\hat{u}_2 + \epsilon^3\bar{u}_2 + \cdots, \\ n_3 = n_3^0 + \epsilon^2\tilde{n}_3 + \cdots, \quad u_3 = \epsilon\hat{u}_3 + \epsilon^3\bar{u}_3 + \cdots. \end{cases} \tag{15}$$

(The moment vector components m_1, m_2 and m_3 are specifically eliminated from the system via Eq. (10) since $u_2^* = u_3^* = 0$.) The use of the Euler angle expansions in Eq. (3) show that the

$$b_i = b_i^0 + \epsilon\hat{b}_i + \epsilon^2\tilde{b}_i + \epsilon^3\bar{b}_i + \cdots \quad (i = 1, 2, 3, 4) \tag{16}$$

with the symmetries

$$\begin{cases} b_0^0 = b_3^0, \quad \hat{b}_0 = \hat{b}_1, \quad \tilde{b}_0 = \tilde{b}_3, \quad \bar{b}_0 = \bar{b}_1, \cdots, \\ b_1^0 = b_2^0, \quad \hat{b}_2 = \hat{b}_3, \quad \tilde{b}_1 = \tilde{b}_2, \quad \bar{b}_2 = \bar{b}_3, \cdots. \end{cases}$$

(The orientation of the Cartesian coordinate system in Fig. 2 has been chosen so as to obtain the same expansion form (16) for all four Euler parameters, which provides a certain ease in developing the perturbation equations.) These expansions are now substituted into the governing equations and boundary conditions to obtain a hierarchy of problems in powers of $O(\epsilon^n)$.

The critical buckling compression $\Delta = L - x(L)$ and the buckling mode are obtained by taking the $O(1)$ and $O(\epsilon)$ equations, which consist, respectively, of the nine nonlinear $O(1)$ equations

$$\begin{cases} (n_2^0)' = u_1^0 n_3^0, \qquad (n_3^0)' = -u_1^0 n_2^0, \qquad (u_1^0)' = n_2^0, \\ (x_0)' = 2(b_1^0 b_3^0 + b_0^2 b_2^0), \qquad (z_0)' = (b_0^0)^2 - (b_1^0)^2 - (b_2^0)^2 + (b_3^0)^2, \\ (b_0^0)' = -b_1^0 u_1^0/2, \qquad (b_1^0)' = b_0^0 u_1^0/2, \qquad (b_2^0)' = b_3^0 u_1^0/2, \qquad (b_3^0)' = -b_2^0 u_1^0/2, \end{cases} \tag{17}$$

and the eight linear, homogeneous $O(\epsilon)$ equations

$$\begin{cases} \hat{u}_2' = (A_3 - 1)u_1^0 \hat{u}_3/A_2 - \hat{n}_1/A_2, & \hat{b}_0' = -(\hat{b}_1 u_1^0 + b_2^0 \hat{u}_2 + b_3^0 \hat{u}_3)/2, \\ \hat{u}_3' = (1 - A_2)u_1^0 \hat{u}_2/A_3, & \hat{b}_1' = (\hat{b}_0 u_1^0 - b_3^0 \hat{u}_2 + b_2^0 \hat{u}_3)/2, \\ \hat{n}_1' = n_2^0 \hat{u}_3 - n_3^0 \hat{u}_2, & \hat{b}_2' = (\hat{b}_3 u_1^0 + b_0^0 \hat{u}_2 - b_1^0 \hat{u}_3)/2, \\ \hat{y}' = 2(b_2^0 \hat{b}_3 + \hat{b}_2 b_3^0 - b_0^0 \hat{b}_1 - \hat{b}_0 b_1^0), & \hat{b}_3' = (-\hat{b}_2 u_1^0 + b_1^0 \hat{u}_2 + b_0^0 \hat{u}_3)/2. \end{cases} \tag{18}$$

The integration of the $O(1)$ equations in terms of elliptic functions and the unknown axial end-load $n_3^0(L)$ is straightforward and can be found in any text considering the large deflection of elastic rods (e.g. Love, 1927). However, for the purpose of computing the buckling mode and the post-buckling behaviour, it is preferable to keep the system as a set of differential equations.

It is straightforward to convert the Euler angle boundary conditions (13) and (14) into ones involving Euler parameters to obtain a set of $O(1)$ boundary conditions

$$\begin{cases} x_0(0) = 0, \qquad b_0^0(0) = b_1^0(0) = b_2^0(0) = b_3^0(0) = 1/2, \qquad n_2^0(0) = 0, \\ z_0(L) = 0, \qquad b_0^0(L) = b_1^0(L) = b_2^0(L) = b_3^0(L) = 1/2, \qquad n_2^0(L) = 0, \end{cases} \tag{19}$$

where the values $z_0(0)$, $u_1^0(0) = \theta_0'(0)$, and $n_3^0(0)$ remain unknown. The $O(\epsilon)$ boundary conditions are

$$\begin{cases} \hat{y}(0) = 0, \qquad -\hat{b}_0(0) = -\hat{b}_1(0) = \hat{b}_2(0) = \hat{b}_3(0) = \hat{\phi}(0)/4 = 1/4, \\ \hat{y}(L) = 0, \qquad \hat{b}_0(L) = \hat{b}_1(L) = \hat{b}_2(L) = \hat{b}_3(L) = 0, \qquad \hat{u}_2(0) = 0, \end{cases} \tag{20}$$

where $\hat{u}_3(0)$ and $\hat{n}_1(0)$ are unknown, and the arbitrary scaling of the $O(\epsilon)$ equations has been set with the choice $\hat{\phi}(0) = 1$.

The solution for the critical compression and the buckling mode for specified dimensionless rigidities A_2 and A_3 is accomplished by a shooting method with $z_0(0)$, $\theta_0'(0)$, $n_3^0(0)$, $\hat{u}_3(0)$, and $\hat{n}_1(0)$ serving as iterates to enforce the five boundary conditions

$$z_0(L) = 0, \qquad b_0^0(L) = 1/2, \qquad \hat{y}(L) = 0, \qquad \hat{b}_0(L) = 0, \qquad \hat{b}_2(L) = 0.$$

The immediate post-buckling behaviour is determined by proceeding with further terms in the ϵ expansion series (15). Because of the odd–even segregation of the various terms, it is necessary to proceed in sets of two terms at a time. The solution of the $O(\epsilon^2)$ and $O(\epsilon^3)$ equations and boundary conditions is detailed in the Appendix A.

Fig. 3 shows a plot of the critical fractional compression Δ/L versus the bending rigidity A_2 for the values of $A_3 = 1.0$, 0.75 and 0.5. The results for the isotropic rod $A_2 = 1$ agree with the results of Miyazaki and Kondo (1997). For large A_2, the critical compression approaches an asymptotic value which is a function of A_3. The asymptotic values associated with $A_3 = 1.0$, 0.75, and 0.5 are 0.8380, 0.7986, and 0.7528, respec-

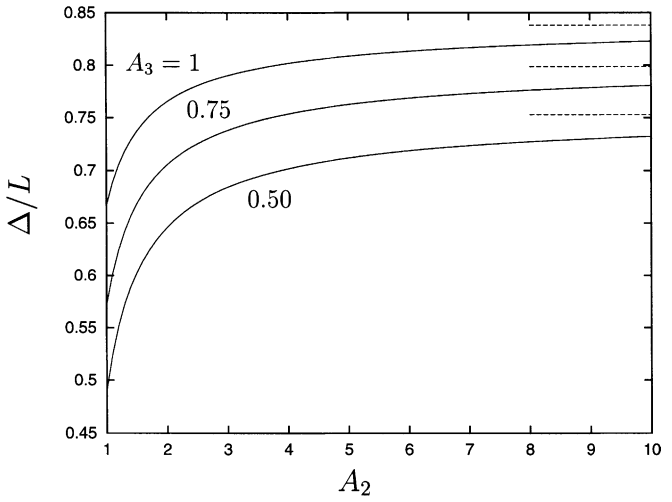

Fig. 3. A plot of the fractional buckling compression Δ/L versus the bending rigidity A_2 for $A_3 = 1$, 0.75, and 0.5. The associated asymptotic values are shown by the straight dash lines.

tively, and are shown by the straight dash lines in Fig. 3. These results are obtained by replacing the $O(\epsilon)$ quantities in Eq. (18) with perturbation expansions in powers of $1/A_2^n$:

$$\hat{n}_1 = \hat{n}_1^\infty + \cdots, \qquad \hat{u}_2 = \hat{u}_2^\infty/A_2 + \cdots, \qquad \hat{u}_3 = \hat{u}_3^\infty + \cdots,$$

and taking the limit $A_2 \to \infty$ to obtain a leading order set of equations for asymptotically large A_2.

The loading behaviours of several typical rods are shown in Fig. 4, where the dimensionless axial pressure $PL^2/EI = -n_3(L)$ has been plotted against the fractional compression Δ/L of the endpoint for

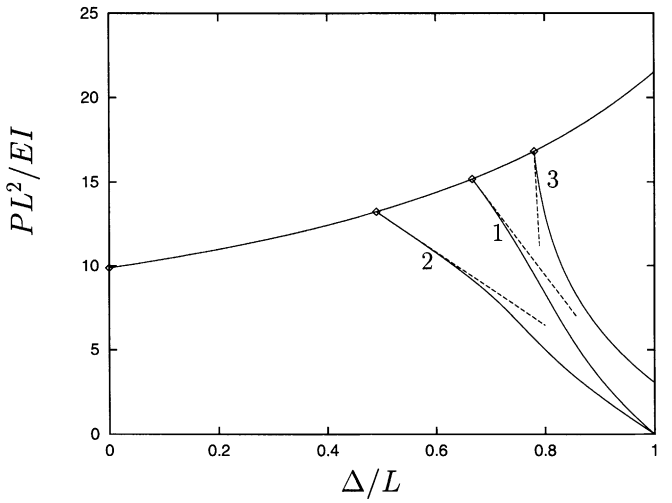

Fig. 4. A plot of the dimensionless axial load PL^2/EI versus the fractional compression Δ/L for several rods. Results shown include the loading path (—) and the approximate post-buckling path (- - -) for the parameter sets $A_2 = A_3 = 1$; $A_2 = 1$, $A_3 = 0.5$; and $A_2 = 10$, $A_3 = 0.75$ (indicated by the numerals 1, 2, and 3).

several sets of A_2 and A_3 values: $A_2 = A_3 = 1$; $A_2 = 1$, $A_3 = 0.5$; and $A_1 = 10$, $A_3 = 0.75$. (The results associated with these sets of parameter values are denoted respectively by the numerals 1, 2, and 3 on the figures of this section.) The solid lines show the solutions (either analytical or numerical) to the full set of nonlinear equations describing the deformation of the straight rods. Buckling into the Euler elastica occurs at the critical load π^2 shown by the small diamond along the vertical axis. Compression initially takes place under a rising load. This curve is given parametrically in terms of the elliptic modulus k ($0 \leqslant k \leqslant 1$) by the expressions

$$\frac{PL^2}{EI} = 4F^2(k) \quad \text{and} \quad \frac{\Delta}{L} = 2 - \frac{2E(k)}{F(k)},$$

where $F(k)$ and $E(k)$ are the complete elliptic integrals of the first and second kinds.

In each case, the Euler elastica solution applies until the compression reaches the critical value (marked by a small diamond) at which point the loading path bifurcates onto the downward sloping solid line, which has been computed from a numerical integration of the full nonlinear equations. The critical compression Δ/L and load values PL^2/EI associated with the above parameter sets are, respectively, (0.6667, 15.186), (0.4902, 13.22), and (0.7804, 16.84). (Beyond the lateral buckling point, the elastica solution is unstable for each of the rods.) After lateral buckling, the axial load drops with increasing compression. The initial response is given approximately by the post-buckling solution developed in the Appendix A, and is indicated by the short straight dash lines of slope -43.07, -21.8, and -592, respectively, for each of the parameter sets mentioned above. For the isotropic rods (numerals 1 and 2), the load drops to zero at a compression of $\Delta/L = 1$, when the rod has deformed into a closed circle with one turn of inserted twist, which is a known stable solution (Zajac, 1962). Note, however, that the anisotropic rod does not deform into a planar circle (although the load goes through zero at some value of Δ/L).

The $O(1)$ rod shapes in the xz-plane and the $O(\epsilon)$ critical buckling mode shapes, as viewed from above looking down at the xy-plane, are shown in Fig. 5 for each of the cases considered in Fig. 4.

4. Buckling of the wound cable

The results for the compression and counter rotation of a wound cable are now presented and can be interpreted in terms of the results of Section 3 in the context of imperfection sensitivity of a straight rod. For simplicity, the dimensionless half length of a helical strand of radius $a = 1$ is taken as $L = 10$, while the overall axial half length of the cable is given by $L\cos\beta$ (Fig. 1). The cable is subject to prescribed axial compression Δz and rotation α about this axis counter to the winding direction.

Fig. 6 shows a plot of the overall dimensionless axial compressive load PL^2/EI versus the fractional axial shortening $\Delta z/L\cos\beta$ for several values of helix angle (all in radians). The limiting case of $\beta = 0$ is described by the dash line and corresponds to a cable composed of two straight rods. This curve is obtained by doubling the single-rod load values of the $A_2 = A_3 = 1$ curve in Fig. 4. Fig. 6 clearly shows classic imperfection sensitivity behaviour with the helix angle β controlling the amplitude of the imperfection. The critical compression associated with the lateral elastica buckling of the straight rod coincides well with the maximum compressive resistance of the wound cable and marks the transition to collapse under a falling load. (Note that the curves in Fig. 4 have been terminated at arbitrary values of compression distance; it is possible to continue the calculations further under falling load.)

Fig. 7 shows a plot of the axial compressive load PL^2/EI versus the axial compression $\Delta z/L\cos\beta$ for a wound cable with the values $\beta = 0.2$ (radians) and $L = 10$ which is subject to counter rotation $\alpha = 0$, 0.2, 0.5, and 1.0 radians. The dash line on Fig. 7 shows the cable which has had no pretwist ($\alpha = 0$) and is

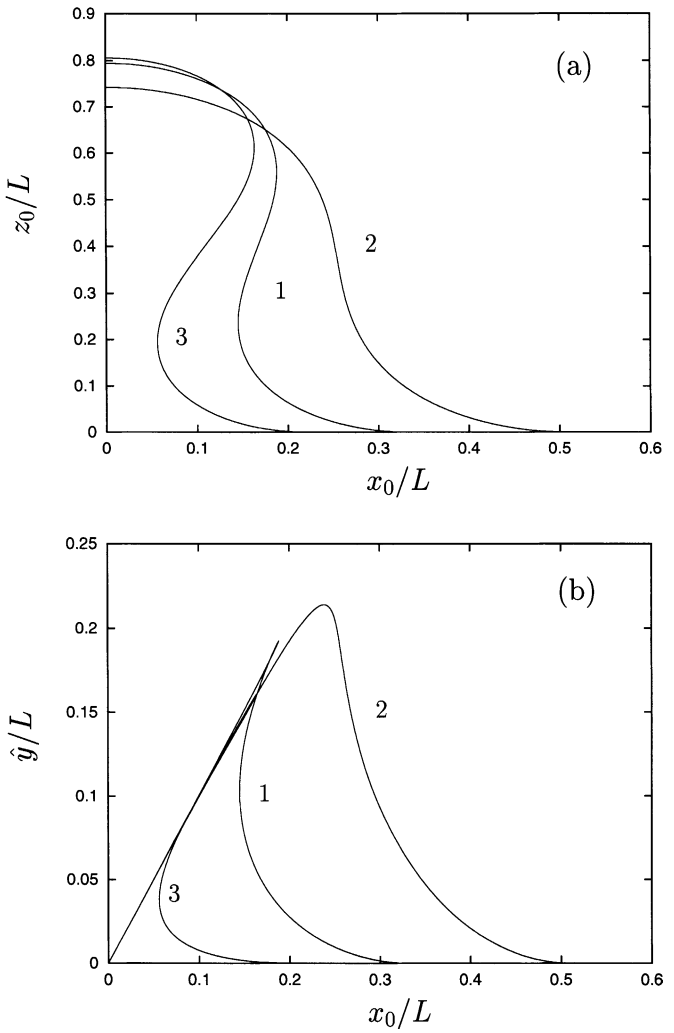

Fig. 5. Critical rod shapes at the point of out-of-plane instability: (a) the leading order xz-plane elastica, and (b) the xy-plane view of the buckling mode. Note that only half solutions are shown. Numerals correspond to those in Fig. 4.

identical to the corresponding β curve in Fig. 6. While counter rotation does not alter the basic behaviour of a rising load followed by a falling load, the effects are more complex when combined with the helical imperfection. For small amounts of compression ($\Delta z/L\cos\beta \leqslant 0.1$), the counter rotation stiffens the cable slightly. This is not unexpected since the strands of the relaxed cable rotate through the angle $L\sin\beta \sim 2.0$ radians about the **k** axis between $s = 0$ and $s = L$. The applied α acts to remove some of this rotation and makes the strands straighter prior to compression so that the cable is initially more rigid.

The behaviour of the cable near the maximum load is more complicated for nonzero α. The small counter rotation $\alpha = 0.2$ stiffens the cable slightly at large fractional compression, but somewhat surprisingly the moderate value of $\alpha = 0.5$ increases the peak load substantially and produces a sharper transition in behaviour. The large value $\alpha = 1.0$ significantly weakens the cable. These trends persist for different values of β and strand lengths L. The pronounced knee present for $\beta = 0.5$ is repeated for different combinations of β and L and presents an enigma at this time.

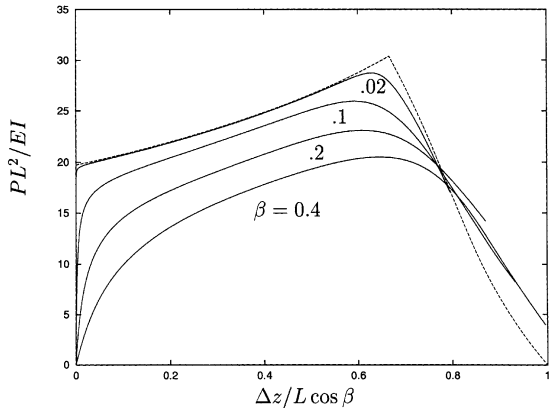

Fig. 6. A plot of the dimensionless axial load PL^2/EI versus the fractional compression $\Delta z/L\cos\beta$ for $L = 10$ and various values of β. The dash line shows the value $\beta = 0$.

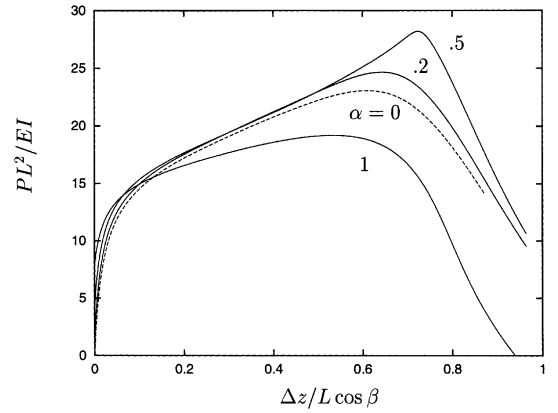

Fig. 7. A plot of the dimensionless axial load PL/EI versus the fractional compression $\Delta z/L\cos\beta$ for $\beta = 0.2$, $L = 10$ and various values of α.

5. Concluding remarks

The birdcaging of wound cables can be understood in terms of the buckling, post-buckling, and imperfection sensitivity of the lateral elastica instability of a straight rod. This study has presented a new method for obtaining both full numerical solutions and post-buckling responses using Euler parameters which remove the numerical difficulties associated with Euler angle formulations.

Acknowledgements

The work of DMS was supported by an Australian Research Council Large Grant while on a sabbatical study leave at the Department of Engineering, Cambridge University. GHMH acknowledges the support from the Royal Society.

Appendix A. The post-buckling response

The leading order post-buckling behaviour must be found by solving the $O(\epsilon^2)$ and $O(\epsilon^3)$ equations in the perturbation expansions. The $O(\epsilon^2)$ system is given by the nine differential equations

$$\begin{cases} \tilde{n}_2' = n_3^0\tilde{u}_1 + \tilde{n}_3 u_1^0 - \hat{n}_1\hat{u}_3, \qquad \tilde{n}_3' = \hat{n}_1\hat{u}_2 - n_2^0\tilde{u}_1 - \tilde{n}_2 u_1^0, \\ \tilde{u}_1' = (A_2 - A_3)\hat{u}_2\hat{u}_3 + \tilde{n}_2, \\ \tilde{x}' = 2(\tilde{b}_1 b_3^0 + b_1^0\tilde{b}_3 + \hat{b}_1\hat{b}_3 + \tilde{b}_0 b_2^0 + b_0^0\tilde{b}_2 + \hat{b}_0\hat{b}_2), \\ \tilde{z}' = \hat{b}_0^2 + 2b_0^0\tilde{b}_0 - \hat{b}_1^2 - 2b_1^0\tilde{b}_1 - \hat{b}_2^2 - 2b_2^0\tilde{b}_2 + \hat{b}_3^2 + 2b_3^0\tilde{b}_3, \\ \tilde{b}_0' = -(\tilde{b}_1 u_1^0 + b_1^0\tilde{u}_1 + \hat{b}_2\hat{u}_2 + \hat{b}_3\hat{u}_3)/2, \\ \tilde{b}_1' = (\tilde{b}_0 u_1^0 + b_0^0\tilde{u}_1 - \hat{b}_3\hat{u}_2 + \hat{b}_2\hat{u}_3)/2, \\ \tilde{b}_2' = (\tilde{b}_3 u_1^0 + b_3^0\tilde{u}_1 + \hat{b}_0\hat{u}_2 - \hat{b}_1\hat{u}_3)/2, \\ \tilde{b}_3' = (-\tilde{b}_2 u_1^0 - b_2^0\tilde{u}_1 + \hat{b}_1\hat{u}_2 + \hat{b}_0\hat{u}_3)/2, \end{cases} \tag{21}$$

while the $O(\epsilon^3)$ system is given by the eight differential equations

$$\begin{cases} \bar{u}_2' = (A_3 - 1)(u_1^0\bar{u}_3 + \tilde{u}_1\hat{u}_3)/A_2 - \bar{n}_1/A_2, \\ \bar{u}_3' = (1 - A_2)(u_1^0\bar{u}_2 + \hat{u}_2\tilde{u}_1)/A_3, \\ \bar{n}_1' = n_2^0\bar{u}_3 + \tilde{n}_2\hat{u}_3 - n_3^0\bar{u}_2 - \tilde{n}_3\hat{u}_2, \\ \bar{y}' = 2(b_2^0\bar{b}_3 + \hat{b}_2\tilde{b}_3 + \tilde{b}_2\hat{b}_3 + \bar{b}_2 b_3^0 - b_0^0\bar{b}_1 - \hat{b}_0\tilde{b}_1 - \tilde{b}_0\hat{b}_1 - \bar{b}_0 b_1^0), \\ \bar{b}_0' = -(\bar{b}_1 u_1^0 + \hat{b}_1\tilde{u}_1 + \tilde{b}_2\hat{u}_2 + b_2^0\bar{u}_2 + \tilde{b}_3\hat{u}_3 + b_3^0\bar{u}_3)/2, \\ \bar{b}_1' = (\bar{b}_0 u_1^0 + \hat{b}_0\tilde{u}_1 - \tilde{b}_3\hat{u}_2 - b_3^0\bar{u}_2 + \tilde{b}_2\hat{u}_3 + b_2^0\bar{u}_3)/2, \\ \bar{b}_2' = (\bar{b}_3 u_1^0 + \hat{b}_3\tilde{u}_1 + \tilde{b}_0\hat{u}_2 + b_0^0\bar{u}_2 - \tilde{b}_1\hat{u}_3 - b_1^0\bar{u}_3)/2, \\ \bar{b}_3' = (-\bar{b}_2 u_1^0 - \hat{b}_2\tilde{u}_1 + \tilde{b}_1\hat{u}_2 + b_1^0\bar{u}_2 + \tilde{b}_0\hat{u}_3 + b_0^0\bar{u}_3)/2. \end{cases} \tag{22}$$

The respective sets of boundary conditions at $s = 0$ are

$$\tilde{x}(0) = 0, \qquad \tilde{n}_2(0) = 0, \qquad \tilde{b}_0(0) = \tilde{b}_1(0) = \tilde{b}_2(0) = \tilde{b}_3(0) = -1/16, \tag{23}$$

and

$$\bar{y}(0) = \bar{u}_2(0) = 0, \qquad \bar{b}_0(0) = \bar{b}_1(0) = -\bar{b}_2(0) = -\bar{b}_3(0) = -\frac{\bar{\phi}(0)}{4} + \frac{1}{96}. \tag{24}$$

The six quantities $\tilde{z}(0)$, $\tilde{u}_1(0)$, $\tilde{n}_3(0)$, $\bar{\phi}(0)$, $\bar{u}_3(0)$, $\bar{n}_1(0)$ serve as iterates in a shooting method and are determined by enforcing the five boundary conditions

$$\tilde{z}(L) = \tilde{n}_2(L) = \tilde{b}_0(L) = \bar{y}(L) = \bar{b}_0(L) = 0,$$

and the additional orthogonality condition

$$\int_0^L \hat{b}_0\bar{b}_0\,\mathrm{d}s = 0$$

between the buckling mode and the higher-order correction (Budiansky, 1974). The simultaneous numerical solution of the Eqs. (21) and (22) is very rapid and is most effectively implemented in conjunction with the numerical procedure to determine the solution of the $O(1)$ and $O(\epsilon)$ equations.

References

Antman, S.S., 1984. Large lateral buckling of nonlinearly elastic rods. Arch. Rational Mech. Anal. 84, 293–305.

Budiansky, B., 1974. Buckling behavior of elastic structures. Adv. Appl. Mech. 14, 1–65.

Champneys, A.R., van der Heijden, G.H.M., Thompson, J.M.T., 1997. Spatially complex localization after one-twist-per-wave equilibria in twisted circular rods with initial curvature. Phil. Trans. R. Soc. Lond. A 355, 2151–2174.

Conway, T.A., Costello, G.A., 1990. Bird-caging in wire rope. J. Eng. Mech. ASCE 116, 822–831.

Costello, G.A., 1978. Analytical investigation of wire rope. Appl. Mech. Rev. 31, 897–900.

Junkins, J.L., Turner, J.D., 1986. Optimal Spacecraft Rotational Maneuvers. Elsevier, Amsterdam.

Kehrbaum, S., Maddocks, J.H., 1997. Elastic rods, rigid bodies, quaternions, and the last quadrature. Phil. Trans. Roy. Soc. Lond. A 355, 2117–2136.

Kovári, K., 1969. Räumliche Verzweigungsprobleme des dünnen elastischen Stabes mit endlichen Verformungen. Ing.-Arch. 37, 393–416.

Landau, L.D., Lifshitz, E.M., 1963. Mechanics. Pergamon, Oxford, pp. 105–115.

Love, A.E.H., 1927. A Treatise on the Mathematical Theory of Elasticity, fourth ed. Cambridge University Press, Cambridge, pp. 381–398 (Chapter 18).

Maddocks, J.H., 1984. Stability of nonlinearly elastic rods. Arch. Rational Mech. Anal. 85, 311–354.

Miyazaki, Y., Kondo, K., 1997. Analytical solution of spatial elastica and its application to kinking problem. Int. J. Solids Struct. 34, 3619–3636.

Nair, S., Hegemeier, G., 1979. Stability of faired underwater towing cables. J. Hydronautics 13, 20–27.

Phillips, J.W., Costello, G.A., 1973. Contact stresses in twisted wire cables. J. Engng. Mech. Div., ASCE 99, Proc. Paper 9676, pp. 331–341.

Zajac, E.E., 1962. Stability of two planar loop elasticas. Trans ASME Ser. E., J. Appl. Mech. 29, 136–142.